Materials Today Chemistry 51 (2026) 103342

Contents lists available at ScienceDirect

Materials Today Chemistry

journal homepage: www.journals.elsevier.com/materials-today-chemistry/

Antibiotic-like properties of cationic linear-dendritic macromolecules having guanidinium peripheral groups

Javier Martín-Martín [a,b], Sara Bescós-Ramo [a,b], Almudena Terrel [a,b], Manuel Arruebo [a,c], Milagros Piñol [a,b], Cristina Yus [a,c,*], Luis Oriol [a,b,**]

[a] Instituto de Nanociencia y Materiales de Aragón (INMA), CSIC-Universidad de Zaragoza, 50009, Zaragoza, Spain
[b] Departamento de Química Orgánica, Facultad de Ciencias, Universidad de Zaragoza, 50009, Zaragoza, Spain
[c] Department of Chemical Engineering and Environmental Technology, Universidad de Zaragoza, 50018, Zaragoza, Spain

ARTICLE INFO

Keywords:
Antibacterial activity
Cytotoxicity
Dendron
Guanidinium
Click chemistry

ABSTRACT

The urgent development of alternatives to conventional antibiotics is essential to address the escalating burden of bacterial antibiotic resistance. Therefore, in this work, we focus on amphiphilic antimicrobial agents having a linear-dendritic structure. They are derived from the first four generations of dendritic polyesters derived from 2,2-bis(hydroxymethyl)propionic acid that are linked to different hydrophobic alkyl chains at the focal point and decorated with cationic guanidinium groups at their periphery. The preparation of these compounds is accomplished through a versatile and orthogonal click chemistry-based strategy. Firstly, alkyl chains are introduced at the focal point of the dendrons via a Cu(I)-catalyzed azide-alkyne cycloaddition. Subsequently, Boc-protected guanidinium groups are attached to the dendron periphery using a thiol-ene reaction, followed by deprotection to yield the cationic guanidinium groups. These amphiphilic linear-dendritic compounds exhibit antimicrobial activity against Gram-positive (*Staphylococcus aureus* ATCC 25923) and Gram-negative (*Escherichia coli* S17) bacteria. The antimicrobial activity and cytotoxicity toward eukaryotic cells, specifically, human dermal fibroblast, HaCaT human keratinocytes and J774A.1 mouse monocyte-macrophages, can be finely optimized to obtain antibiotic-like materials by varying the dendritic generation and adjusting the hydrophobic/hydrophilic balance, which is mainly governed by the length of the alkyl chain at the focal point of the dendron. The orthogonal click chemistry strategy enables facile modulation of the hydrophobic/hydrophilic balance from a common dendritic scaffold, achieving a linear-dendron agent that displays antimicrobial activity comparable to that of conventional antibiotics, while maintaining high cytocompatibility.

1. Introduction

The increasing resistance of pathogenic bacteria to conventional antibiotics, fueled by their widespread misuse and the limited discovery of new antibiotics, represents an escalating threat to global health [1–3]. Therefore, there is a pressing need to develop new antimicrobial candidates that prevent or hinder the generation of antimicrobial resistance. Antimicrobial peptides (AMPs), also known as host-defense peptides, have emerged as promising alternatives to traditional antibiotics [4,5]. AMPs are typically composed of 10–50 cationic amino acids and present an amphiphilic structure, being the balance between cationic and hydrophobic residues essential for their antimicrobial activity. The cationic groups of AMPs electrostatically interact with the anionic components of the bacterial membrane and the hydrophobic residues fuse with the phospholipid bilayer of the plasma membrane. These non-specific interactions compromise membrane integrity, leading to permeabilization, disruption, and ultimately, cell death [6,7]. Besides, the antimicrobial resistance is generally less frequent or more slowly developed than in the case of traditional antibiotics due to these non-specific interactions between AMPs and bacterial membranes [8]. Despite their potent and broad-spectrum antimicrobial activity and reduced risk of inducing resistance, AMPs also present several drawbacks, including high production costs, low physiological stability, and significant toxicity to mammalian cells [9–11]. However, these limitations can be addressed through the design and synthesis of versatile AMP-mimetic polymers [12].

* Corresponding author. Instituto de Nanociencia y Materiales de Aragón (INMA), CSIC-Universidad de Zaragoza, 50009, Zaragoza, Spain.
** Corresponding author. Instituto de Nanociencia y Materiales de Aragón (INMA), CSIC-Universidad de Zaragoza, 50009, Zaragoza, Spain.
E-mail addresses: cyargon@unizar.es (C. Yus), loriol@unizar.es (L. Oriol).

https://doi.org/10.1016/j.mtchem.2025.103342
Received 10 September 2025; Received in revised form 27 December 2025; Accepted 30 December 2025
Available online 2 January 2026

To date, a wide range of antimicrobial cationic synthetic polymers have been developed, mostly based on non-degradable linear backbones, such as polymethacrylates [13,14]. To avoid side health effects of non-degradable polymeric chains, antimicrobial degradable synthetic polymers like aliphatic polycarbonates [15,16] or polyesters [17], containing cationic groups, have also been described. Concerning the cationic functionalization, several groups have been explored, being ammonium and guanidinium groups the most common [18,19]. In particular, guanidinium groups, which structurally resemble arginine residues, have demonstrated enhanced antimicrobial efficacy compared to their ammonium-containing counterparts, as reported in several studies for synthetic linear polymers [16,20]. The hydrophobic/hydrophilic balance is also a determinant factor for the effectiveness of these AMP-mimetic synthetic polymers against bacteria, as directly influences the disruption of lipidic membranes. In most cases, increasing the hydrophobic balance enhances the antimicrobial activity of polymers but compromises their biocompatibility and solubility [21,22]. Consequently, significant efforts have been made to optimize the nature of cationic charges, the amphiphilic balance, and the chemical structure to obtain polymers exhibiting strong antimicrobial activity and high biocompatibility [23].

Compared to linear antimicrobial polymers, dendrimers have been less studied, although their monodispersity and well-defined architecture might offer better control and reproducibility of antimicrobial and hemolytic activities [24]. Among the different explored dendrimers as antimicrobial macromolecules [25–28], aliphatic polyester-based dendrimers stand out due to their demonstrated degradability under physiological conditions, which results in a reduced toxicity [29]. In this regard, Stenström et al. reported a series of dendrimers based on 2,2-bis (hydroxymethyl)propionic acid (bis-MPA), functionalized, via esterification of the peripheral hydroxyl groups, with ammonium moieties and spanning generations from one to five [30]. In later work, the same group incorporated ammonium groups using cysteamine and a thiol-ene reaction to decorate the dendron periphery. This process produced thioether bonds rather than hydrolysable esters, which increased dendrimer stability under physiological conditions and led to higher antimicrobial efficacy without a significant rise in cytotoxicity against monocyte/macrophage-like cells and human dermal fibroblasts [31].

Amphiphilic dendronized macromolecules, particularly those with a linear-dendritic structure, constitute an interesting alternative to dendrimers. Their design allows precise tuning of the hydrophobic/hydrophilic balance by incorporating hydrophobic entities at the focal point of the dendron, while the charge density can be modulated by varying the dendritic generation, thus optimizing both antimicrobial activity and cytotoxicity [26,28,32–36]. Motivated by the role of some fatty acid chains in many AMPs, Siriwardena et al. synthesized a peptide dendron featuring a linear lipid chain and ammonium cationic groups, resembling an amphiphilic dendron-tail structure. This macromolecule exhibited remarkable antimicrobial effects against *Pseudomonas aeruginosa* PAO1 and *Escherichia coli* DH5α, with minimum inhibitory concentrations (MICs) as low as 3 and 1 μg/mL, respectively [37]. The importance of combining a dendritic structure and linear aliphatic tails in AMPs was also corroborated by Lai et al. having in this case guanidinium as cationic groups [38].

However, the synthesis of amphiphilic dendritic-like AMPs is challenging. Synthetic dendrons having linear aliphatic tails have been explored mainly based on poly(amidoamine) (PAMAM) dendrons as a more versatile alternative than synthetic peptides with dendritic structure. Guo et al. described the first two generations of amphiphilic PAMAM dendrons, having peripheral ammonium cationic groups and aliphatic tails connected to a focal point. The MICs exhibited by these dendrons for several Gram-positive and Gram-negative bacteria decreased when the aliphatic tail was increased [28]. Dhumal et al. described a series of amphiphilic linear-dendritic macromolecules based on a PAMAM dendron of third-generation connected to an aliphatic tail, with self-assembly properties [34]. Different ionic groups were introduced at the dendron periphery and the authors observed that the ammonium groups exhibited potent antimicrobial activity (MIC = 6 μg/mL for *Escherichia coli* CECT 515), whereas, surprisingly, the guanidinium groups were poorly active (MIC = 200 μg/mL for *Escherichia coli* CECT 515), despite having shown similar or improved activity than ammonium groups in dendrimers with the same chemical structure [32]. The resulting ammonium amphiphilic PAMAM dendrons were evaluated *in vivo* in murine models and did not induce resistance against *Escherichia coli* MG1655 and *A. baumannii* ATCC17978, being an alternative to target antibiotic-resistant bacterial pathogens [39,40].

Bis-MPA polyester dendrons have been scarcely investigated in the emerging field of amphiphilic linear-dendritic antimicrobial molecules [33], despite the antimicrobial activity exhibited by high generations of this type of dendrons [27,41,42]. Chen et al. reported amphiphilic bis-MPA dendrons up to the third-generation, functionalized with ammonium groups at the periphery and alkyl chains of different lengths (from 2 to 14 carbon atoms) at the focal point as hydrophobic tails, designed to function as antimicrobial agents. By adjusting the dendritic generation and the alkyl chain length, an optimal balance between antimicrobial activity and cytotoxicity was achieved. The generation number primarily influenced the cytotoxicity, decreasing at higher generations, while the length of the focal alkyl chain affected the antimicrobial activity, increasing with longer alkyl chains. Therefore, an optimal balance between hemolytic and antimicrobial activity was achieved for the third-generation dendron combined with the longest alkyl chain having 14 carbon atoms [35]. In a subsequent study, the same authors synthesized comparable linear-dendritic structures but with peripheral guanidinium groups [36]. As observed in the aforementioned ammonium dendrons, antimicrobial activity increased with the alkyl chain length, while cytotoxicity decreased with higher dendritic generations. However, all compounds showed similar values in antimicrobial activity or cytotoxicity to their ammonium counterparts. Nevertheless, this study was limited to the first two dendron generations, as higher generations could not be successfully synthesized, in contrast to what previously reported for ammonium analogs.

Building on the previous works, the present study describes the synthesis, antimicrobial activity and cytotoxicity of guanidinium functionalized bis-MPA dendrons up to the fourth-generation with different alkyl chains at the focal point. Bis-MPA is a building block with excellent synthetic versatility to prepare biodegradable dendrons with low toxicity in comparison to other dendritic materials, such as PAMAM [29,30]. In these systems, the best balance of dendron generation and/or aliphatic tail length was evaluated to obtain antimicrobial agents with low cytotoxicity against eukaryotic cells. To achieve higher dendron generations, a versatile and efficient orthogonal click functionalization strategy was devised, employing allyl-functionalized dendron precursors with an azido group at the focal point. This approach first involves attaching alkyl chains at the focal point via Cu(I)-catalyzed azide-alkyne cycloaddition (CuAAC), followed by the introduction of guanidinium groups at the periphery of the dendron scaffold through a thiol-ene light-initiated reaction. This approach is highly versatile as the hydrophobic/hydrophilic balance can be adjusted just by clicking preformed dendrons and aliphatic tails. Finally, the cationic groups were connected to the resulting platform to modulate the charge density at the surface. Antimicrobial activity was evaluated against *Staphylococcus aureus* ATCC 25923 and *Escherichia coli* S17 as representative models of Gram-positive and Gram-negative bacteria, respectively. Besides, cytotoxicity studies were conducted on several eukaryotic cells, including keratinocytes (HaCat), fibroblasts, and macrophages.

2. Materials and methods

2.1. Materials

6-Azidohexan-1-ol and compounds **(1)**, **(2)** and **(3)** were synthesized according to previously reported procedures [43,44]. Tryptic Soy Broth

(TSB) was purchased from Condalab (Spain) and Tryptic Soy Agar (TSA) plates made using Chromocult® dehydrated media produced byMerck KGaA (Germany). Paraformaldehyde 4 % in PBS was obtained from Alfa Aesar (Germany). Dulbecco's Phosphate Buffered Saline (DPBS), Dulbecco's modified Eagle's medium high glucose with stable glutamine (DMEM) and antibiotic-antimycotic solution (penicillin-streptomycin-amphotericin B; PSA) were acquired from Biowest (France). Fetal bovine serum (FBS) was purchased from Gibco (USA), and the Blue Cell viability assay kit was supplied by Abnova (Taiwan). All other reagents and solvents were purchased from Sigma-Aldrich and Fisher Scientific and were used as received.

2.2. Characterization techniques

ICP-OES analysis was carried out on a Thermo Scientific I CAP PRO XP Duo spectrometer. Infrared (IR) spectra were recorded on a Bruker Vertex 70 spectrophotometer using 1–2 % (w/w) KBr pellets. ^{1}H nuclear magnetic resonance (^{1}H NMR), ^{13}C NMR and ^{19}F NMR spectra were registered on a Bruker AV-400 spectrometer using either $CDCl_3$, DMSO-d_6 or CD_3OD. Matrix-assisted laser desorption ionization, time-of-flight mass spectrometry MALDI-TOF MS was performed on an Autoflex Bruker mass spectrometer using dithranol as matrix. High resolution mass spectrometry (HRMS) was carried out in a positive ion electrospray ionization (ESI+) mode on a Bruker Q-TOF-MS instrument. Dynamic light scattering (DLS) measurements were carried out in a Malvern Instrument Nano ZS using a He–Ne laser with a 633 nm wavelength and a detector angle of 173° at 25 °C. The size measurements were registered three times to ensure reproducibility. Transmission Electron Microscopy (TEM) was carried out on a FEI TECNAI T20 electron microscope operating at 200 kV. The fluorescence measurements to determine the CAC of the self-assemblies were conducted on a PerkinElmer LS 50B fluorescence spectrophotometer. Fluorescent measurements for *in vitro* cytotoxicity assays were performed in a Varioskan LUX microplate reader (Thermo Fisher, USA). The morphology of bacteria was observed by an Inspect F50 field emission gun scanning electron microscope (FEI Company, USA).

2.3. Synthesis

2.3.1. General procedure for CuAAC reaction in the preparation of *m-Gn-All*

CuBr (20 % mol with respect to dendron) and *N*,*N*,*N*′,*N*″,*N*″-pentamethyldiethylenetriamine (PMDETA) (20 % mol with respect to dendron) were added to a solution of **Az-Gn-All** and alkyne compound (20 % excess of alkyne group with respect to azide) in DMF (approx. ratio 2-1 mL per 100.0 mg of **Az-Gn-All**) previously purged and deoxygenated with argon. The reaction was stirred for 24 h at RT and then, concentrated under vacuum. The crude was dissolved into DCM (20 mL) and washed with water (5 × 20 mL). The organic layer was dried over $MgSO_4$, filtered, and evaporated. **1-Gn-All** required no further purification, as hex-1-yne was removed during evaporation. In contrast, **2-Gn-All** were further purified by flash column chromatography on silica gel, as indicated in the Supporting Information. The characterization data of all **m-Gn-All** are provided in the Supporting Information.

2.3.2. General procedure for the thiol-ene reaction in the preparation of *m-Gn-Boc*

2,2-Dimethoxy-2-phenylacetophenone (DMPA) (5 % mol with respect to allyl groups) was added to solution of **m-Gn-All** and **GuBoc-SH** thiol (100 % mol excess of thiol with respect to allyl groups) in THF (approx. ratio 1 mL per 100 mg of **m-Gn-All**), previously purged and deoxygenated with argon. Then, the reaction was irradiated at 365 nm, using a Philips PL-S-9W UV Hg lamp, while stirring at RT for 6 h. The solvent was evaporated under vacuum. The first- and second-dendron generations were purified by flash column chromatography, employing mixtures of hexane/AcOEt as eluents. The third- and fourth-dendron generations were purified by precipitation in cold MeOH or by preparative size exclusion chromatography (SEC) employing Bio-beads SX-1 and THF as eluent, depending on the kind of dendron, as indicated in the Supporting Information. The characterization data of all **m-Gn-Boc** are provided in the Supporting Information.

2.3.3. General procedure for the Boc deprotection in the preparation of *m-Gn*

A solution of **m-Gn-Boc** in a mixture of DCM/trifluoroacetic acid (TFA) (9:1) (approx. 10 mL per 150 mg of **m-Gn-Boc**) was prepared and stirred at RT for 6 h. Afterwards, the solvent was removed by vacuum and the crude was precipitated in cold diethyl ether. Then, the dendron was dissolved in Milli-Q® water and lyophilized. The characterization data of all **m-Gn** are provided in the Supporting Information.

2.4. Determination of the critical aggregation concentration (CAC)

CAC was determined by fluorescence spectroscopy using Nile Red as polarity sensitive probe. A solution of Nile Red in DCM at a concentration of 6.0×10^{-6} M was prepared. Then, 100 μL of this solution were added to a vial, and the solvent evaporated at RT for 6 h. Subsequently, 600 μL of the self-assembly dispersion, with concentrations ranging from 1.0×10^{-4} to 1.0 mg/mL, were added into the vial, achieving a final Nile Red concentration of 1.0×10^{-6} M. The mixture was then stirred overnight in an orbital shaker. Finally, the emission spectra of Nile Red solution were registered from 530 to 900 nm while exciting at 550 nm.

2.5. Bacterial culture

Staphylococcus aureus ATCC 25923 (*S. aureus*), obtained from Ielab (Spain), was used as a model of Gram-positive bacteria and *Escherichia coli* S17 (*E. coli*), kindly donated by Dr. Jose A. Ainsa (University of Zaragoza, Spain), was selected as a model of a Gram-negative one. A colony of each strain was cultured in TSB at 37 °C under continuous shaking for 24 h, until stationary phase growth ($\sim 10^9$ CFU/mL) was reached.

2.6. In vitro antibacterial activity

Different concentrations of each of the 8 compounds were tested against both bacterial strains to determine the MIC and the Minimal Bactericidal Concentration (MBC). Briefly, bacteria were diluted to 10^5 CFU/mL and exposed to the different compounds in TSB and incubated at 37 °C under continuous shaking (150 rpm) for 24 h. To quantify viable bacteria, the standard microdilution method was performed on TSA plates. Their effectiveness was assessed under the same experimental conditions to ensure reliable comparisons with the tested compounds. Untreated bacteria were used as negative control. After 24 h of incubation for the agar plates at 37 °C, bacteria colonies were counted. Each experiment was conducted with three independent biological replicates in triplicate.

For scanning electron microscopy (SEM) evaluation of membrane damage, bacteria were incubated with each of the tested compounds at their corresponding MICs. After 24 h of incubation, bacteria were centrifuged for 5 min at 3000 rpm and the supernatant was replaced with PFA for bacteria fixation and kept for 24 h. Afterwards, samples were washed twice with PBS 1x and dehydrated with a series of ethanol gradients in duplicate, the samples were left to air dry. Prior to electronic visualization, bacterial samples were coated with Pd.

2.7. In vitro cytotoxicity assay

Human dermal fibroblasts (NHDF-Ad) were obtained from Lonza (Basel, Switzerland), HaCaT human keratinocytes were kindly donated by Dr. Pilar Martín-Duque (University of Zaragoza, Spain) and J774A.1 mouse monocyte-macrophages ATCC-TIB-67™ were obtained from LGC

Standards (Barcelona, Spain). All cell lines were cultured in high-glucose DMEM with stable glutamine, supplemented with 10 % (v/v) FBS and 1 % (v/v) PSA, incubated at 37 °C in an atmosphere with 5 % CO_2.

The cytotoxicity assay for the different compounds was conducted using the Blue Cell Viability Assay following the manufacturer's instructions. Briefly, 6000 cells per well were seeded and incubated for 24 h at 37 °C in a 5 % CO_2 atmosphere. Then, the compounds were added at different concentrations and, after 24 h of incubation, the alamarBlue Cell Viability reagent was added at 10 % (v/v). After 4 h at 37 °C and 5 % CO_2, fluorescence was measured at 530/590 ex/em in a

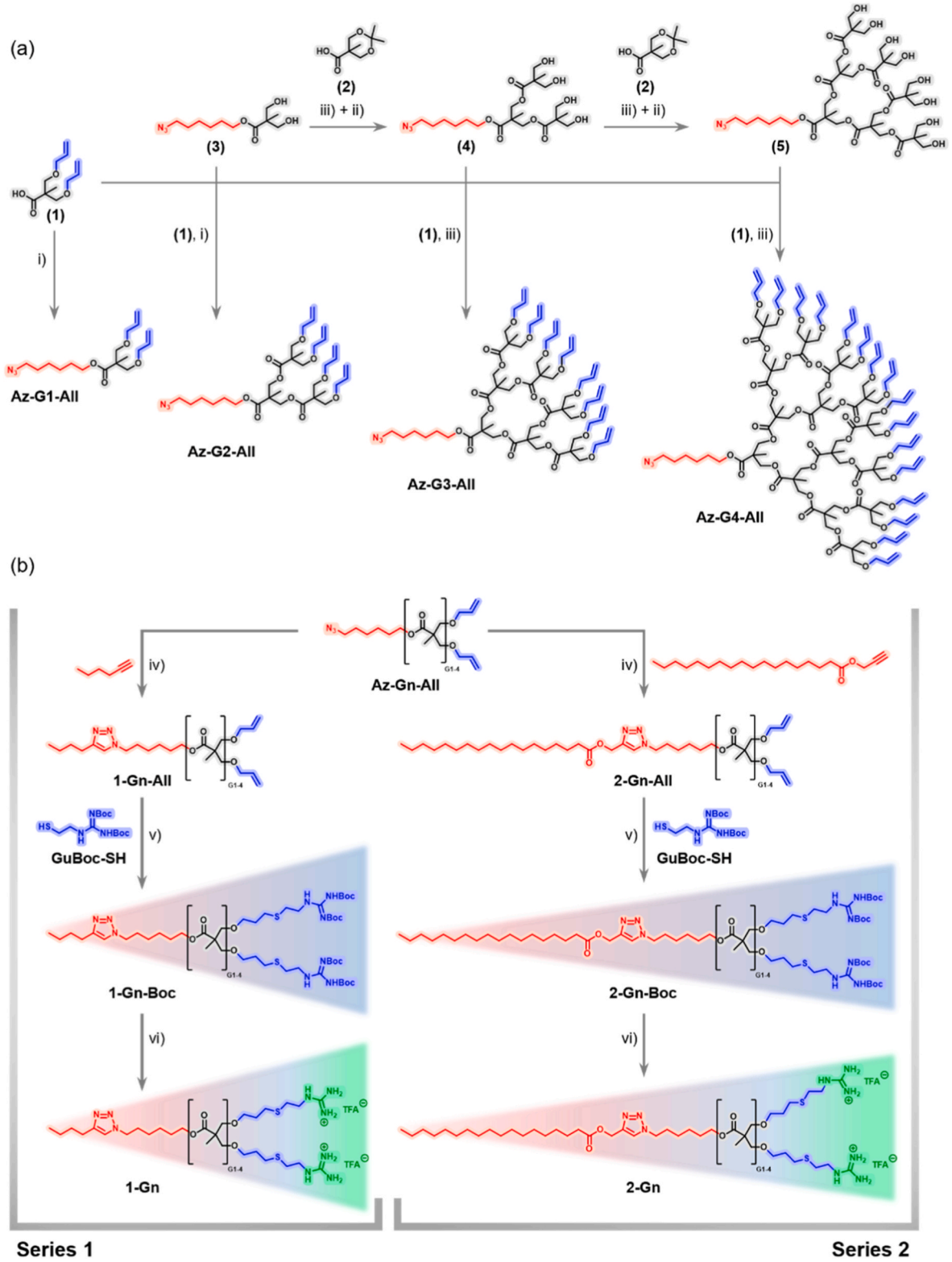

Scheme 1. **(a)** Synthesis of **Az-Gn-All** dendrons. Reaction conditions: **i)** DCC/DPTS, anhydrous DCM, **ii)** Dowex® 50WX2 resin, MeOH, **iii)** CDI/CsF, AcOEt. **(b)** Synthesis of **1-Gn** and **2-Gn** series. Reaction conditions: **iv)** CuBr, PMDETA, DMF, **v)** DMPA, DMF, UV light, and **vi)** TFA, DCM. (See experimental procedures in Supporting Information).

microplate reader. Untreated cells were considered as control samples. Cellular cytotoxicity was assessed by comparing the measurements from treated cells to those obtained from untreated controls, which were considered to have 100 % viability. Each experiment was conducted with three independent biological replicates, each measured in triplicate. The cytotoxicity of each compound was used to determine the IC_{50} values, defined as the concentration required to reduce cell viability by 50 %. IC_{50} values were calculated from dose–response curves obtained using nonlinear regression analysis. To evaluate the therapeutic potential and safety margin of each compound, the selectivity index (SI) was calculated as the ratio between the IC_{50} value and the corresponding MIC value ($SI = IC_{50}/MIC$). The SI provides a measure of how a compound inhibits selectively microbial growth relative to its cytotoxicity toward mammalian cells. Compounds with higher SI values are considered more selective towards bacteria and therefore more promising for further development, as they display antimicrobial activity at concentrations lower than those causing cytotoxic effects on eukaryotic cells.

3. Results and discussion

3.1. Synthesis and characterization of guanidinium dendrons

Series of guanidinium-modified linear-dendritic macromolecules were synthesized from preformed dendrons ranging from the first-to the fourth-generation (**Az-Gn-All**, where *n* is the dendron generation).

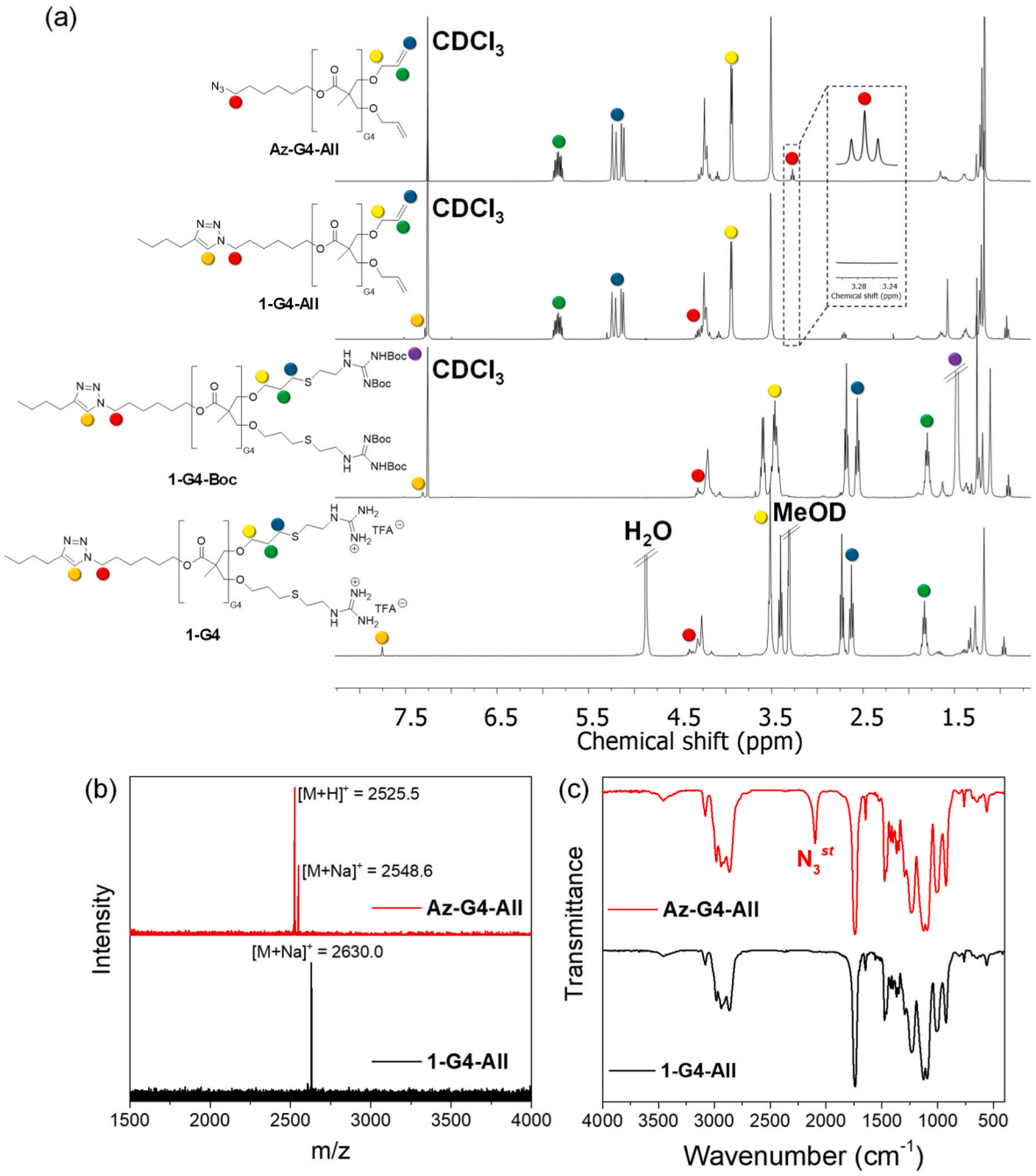

Fig. 1. (a) ^1H NMR (400 MHz, $CDCl_3$) spectra of **Az-G4-All**, **1-G4-All** and **1-G4-Boc** dendrons and ^1H NMR (400 MHz, CD_3OD) spectra of **1-G4** dendron. The inset image shows the amplified signal of the methylenic protons attached to the azido group. **(b)** MALDI-TOF MS results of **Az-G4-All** and **1-G4-All**, using dithranol as matrix. **(c)** FTIR spectra of **Az-G4-All** and **1-G4-All**.

These dendrons contain an azido group at the focal point, acting as a clickable site to attach an aliphatic tail and 2^n allylic peripheral groups (n, dendron generation), serving as clickable sites for the introduction of guanidine-derived thiols in an orthogonal and versatile manner (Scheme 1). The **Az-Gn-All** dendrons were prepared using a divergent strategy, as depicted in Scheme 1a, from three elemental bis-MPA building blocks. First, the allyl functionalized bis-MPA **(1)**, which forms the periphery of the dendron and serves as the precursor for the dendron of generation $n = 1$. Second, the acetonide protected bis-MPA **(2)**, employed to build the inner structure of dendron. Third, the azide functionalized bis-MPA derivative **(3)**, prepared from **(2),** which enables the attachment of aliphatic tails to the focal point of dendrons of generations $n = 2$–4. The first-generation dendron, **Az-G1-All**, was obtained by esterification of **(1)** with 6-azidohexan-1-ol under Steglich conditions, using *N*,*N*′-dicyclohexylcarbodiimide (DCC) and 4-(dimethylamino)pyridinium 4-toluenesulfonate (DPTS). The second-generation dendron, **Az-G2-All**, was similarly synthesized by an esterification reaction using **(1)** and **(3)** as building blocks. For the synthesis of third- and fourth-generation dendrons, **Az-G3-All** and **Az-G4-All**, building blocks **(2)** and **(3)** were first used to grow the dendron generation using iterative esterification and acetonide deprotection to yield **(4)** and **(5)** having hydroxyl groups at the periphery. Dendrons, **Az-G3-All** and **Az-G4-All**, were eventually prepared by Fluoride-Promoted Esterification (FPE) of the peripheral hydroxyl groups with the building block **(1)** using cesium fluoride and carbonyldiimidazole (CDI) to activate the carboxylic group. This modification in the esterification process enabled an easier access to higher generation dendrons with shorter reaction times, and a simplified work-up [45]. All intermediates were fully characterized, in particular to ensure the formation of defect-free dendrons. Well-defined **Az-Gn-All** dendritic scaffolds were identified by ^{1}H NMR and MS. As an example, the ^{1}H NMR spectrum of **Az-G4-All** is shown in Fig. 1a, where signal intensities confirmed the presence of 16 allyl groups at the dendron periphery. This was further supported by the corresponding mass spectrometry results, which displayed only two distinct molecular m/z peaks at 2525.5 and 2548.6, attributed to the protonated and sodiated **Az-G4-All** species, respectively, with no additional peaks which could indicate an incomplete esterification (Fig. 1b).

Two series of guanidinium dendronized macromolecules, **1-Gn** and **2-Gn**, were prepared through sequential click reactions on the **Az-Gn-All** scaffolds (Scheme 1b). First, an alkyl chain was connected to the dendron by CuAAC of the azide with either hex-1-yne (series **1-Gn**) or propargyl stearate (series **2-Gn**) using CuBr and PMDETA in DMF, with a slight excess of the alkyne. Next, the peripheral allyl groups were functionalized with the Boc-protected guanidine thiol, **GuBoc-SH**, by a UV-light-initiated thiol-ene reaction using DMPA as a radical UV photoinitiator, and with a two-fold excess of **GuBoc-SH** to facilitate the complete peripheral functionalization. The cationic guanidinium-functionalized dendrons were obtained by removing the Boc groups with TFA. The specific sequential order of these reactions was strategically designed to ensure optimal reaction conditions, selectivity and product integrity. Thus, CuAAC was performed first because the azido group selectively and orthogonally reacts with the terminal alkyne in the presence of allyl groups, ensuring high efficiency and regioselectivity. Initiating the process with thiol-ene modification at the periphery was ruled out due to the potential degradation of azides into nitrenes under UV light [46], which could compromise the integrity of the dendron focal point. Furthermore, conducting CuAAC in the presence of Boc-protected guanidine groups was deliberately avoided, as guanidine moieties can coordinate with Cu(I) ions, reducing reaction efficiency and complicating subsequent purification steps.

The CuAAC proceeded quantitatively according to NMR, Fourier Transform Infrared (FTIR) spectroscopies, and MS (Fig. S36–43). Using the G4 dendron from series 1 as a representative example, the ^{1}H NMR spectrum revealed a downfield shift of the methylene protons directly attached to the azido group, from 3.27 ppm (Fig. 1a, inset) to 4.33–4.15 ppm, attributed to the proton of the triazole ring in the click adduct, confirming the successful completion of the coupling reaction. The ^{13}C NMR spectrum also showed two signals at 148.5 and 120.6 ppm corresponding to triazole ring (Fig. S1). MALDI-TOF MS characterization also verified the coupling since only a single molecular m/z peak was observed, further supporting the completion of the reaction and confirming the purity of the final product (Fig. 1b). Likewise, FTIR spectroscopy also supported the completion of the click reaction by the disappearance of azide stretching band of **Az-G4-All** dendron at approx. 2100 cm^{-1} (Fig. 1c).

The functionalization of allyl groups with **GuBoc-SH** thiols was tracked by ^{1}H NMR (Fig. 1a). As the reaction progressed, the intensity of ^{1}H NMR allyl protons at 3.94, 5.28-5.08 and 5.90–5.78 ppm decreased, while new signals emerged attributed to the formed trimethylene spacer. Consistently, the ^{13}C NMR spectrum also confirmed the disappearance of double bond protons along with the appearance of signals corresponding to the Boc-protected guanidine groups (Fig. S1). The removal of Boc protecting groups was monitored by ^{1}H NMR by the disappearance of Boc signal at 1.30–1.60 ppm. As an example, Fig. 1a shows the ^{1}H NMR spectrum of **1-G4**. Similarly, the disappearance of Boc methyl carbons in the ^{13}C NMR spectrum was also checked (Fig. S1). The presence of free TFA in the final guanidinium linear-dendritic compounds was ruled out by recording the ^{19}F NMR spectrum. Thus, in **1-G4** a single peak at −76.9 ppm, corresponding to the trifluoroacetate anion, was recorded and no evidence of an additional signal at −77.9 ppm, which would indicate the presence of free TFA, was detected (Fig. S2) [47].

The presence of copper in the final compounds was evaluated using inductively coupled plasma optical emission spectroscopy. Copper levels, if present, were below the minimum detectable concentration of the technique. In conclusion, using this versatile approach based on complementary click reactions, guanidinium-containing amphiphilic linear-polyester dendron compounds can be successfully prepared, including high dendron generations, with complete peripheral functionalization.

3.2. Antibacterial activity

The antimicrobial activity of these linear-dendritic macromolecules was assessed in Gram-positive (*Staphylococcus aureus*) and Gram-negative (*Escherichia coli*) bacteria in order to determine the MIC and MBC by the serial dilution method. The data obtained are compiled in Table 1. The selected bacterial strains were chosen to explore whether differences in the observed bactericidal activity could be dependent on the different bacterial membrane composition and charge.

It was found that **1-Gn** compounds exhibited bactericidal effects at significantly lower concentrations compared to their **2-Gn** counterparts. As the length of the alkyl chain linked to triazole ring increased from 4 to 19 carbon atoms, the compounds became more hydrophobic, which appeared to hinder their effective interaction with the bacterial

Table 1
Bactericidal activity of linear-dendritic compounds against Gram-positive *S. aureus* and Gram-negative *E. coli* strains. At least three independent replicates were performed in triplicate.

Dendron	MIC (μg/mL)		MBC (μg/mL)	
	S. aureus ATCC 25923 (Gram-positive)	*E. coli* S17 (Gram-negative)	*S. aureus* ATCC 25923 (Gram-positive)	*E. coli* S17 (Gram-negative)
1-G1	2.5	20–50	20	50
1-G2	2.5	2.5	5	5
1-G3	10	5	20	10
1-G4	100	20	200	100
2-G1	250	>500	500	>500
2-G2	50–100	100–150	150	150
2-G3	150	50	500	100
2-G4	250–500	250	>500	500

membrane. Specifically, **1-G1** compound inhibited the growth of *S. aureus* at a concentration of 2.5 μg/mL and *E. coli* at concentrations ranging from 20 to 50 μg/mL. In contrast, the longer-chain compound, **2-G1**, inhibited *S. aureus* growth at 250 μg/mL and *E. coli* at 500 μg/mL, representing at least a tenfold increase in the required concentration.

This decrease in antibacterial activity with increasing chain length may be attributed to the reduced solubility and increased steric hindrance, which can impair their ability to interact and disrupt the bacterial membranes. Additionally, excessive hydrophobicity might lead to stronger self-aggregation in aqueous environments, further reducing the surface-to-volume ratio and the consequent bioavailability of the compound. The relationship between alkyl chain length and antibacterial activity was reported to be associated with the ability of the alkyl chains to fuse to the bacterial membranes, leading to membrane disruption [48]. Similar mechanisms were recently described by Hanheiser et al., who observed enhanced antimicrobial effects when employing amphiphilic intermediate dendron generation of oligoglycerols having four peripheral ammonium groups with a short aliphatic chain linked to the focal point (two lengths were studied), and attributing this improved activity not only to a better solubility and membrane accessibility but also to a more favorable balance between hydrophobic and hydrophilic domains [49]. However, other linear-dendrons based on bis-MPA, functionalized with ammonium or guanidinium groups at the periphery, exhibited an opposite trend in antimicrobial activity, a longer aliphatic chain at the focal point enhanced the antimicrobial effect [35, 36]. Therefore, the correlation between alkyl chain length and antibacterial activity remains unclear due to non-linear behavior, the multiple biological and chemical variables involved, and system-dependent effects.

On the other hand, within the same alkyl chain length, specifically in the **1-Gn** series compounds, it was observed that for both bacterial strains the MICs required to inhibit bacterial growth followed an increasing trend for higher generations of the guanidinium compound. The compound demonstrating the most promising antibacterial activity was **1-G2**, with a MIC of 2.5 μg/mL and a MBC of 5 μg/mL for both *S. aureus* and *E. coli*. This compound exhibited stronger bactericidal activity than both its lower generation counterpart, **1-G1**, and higher generation analogs, **1-G3** and **1-G4**, whose antimicrobial concentrations increased by one to two orders of magnitude. This behavior may be attributed to a balance between the increased number of positive charges introduced by additional guanidinium groups, enhancing the electrostatic interaction with the negatively charged bacterial membranes, and the potential steric hindrance associated with the incorporation of bulkier structures [50]. These results are consistent with the findings reported in the recent literature, where an increase in the number of positively charged groups from 2 to 4 led to enhanced bactericidal activity. However, when the number of guanidinium groups increased to 8, the bacterial growth was observed to rise again at the same inhibitory concentrations [49]. Also, the self-assembly properties of these dendrons can contribute to bactericidal activity. The formation of self-assembled nanostructures in water was studied by DLS and TEM for **1-G2**, which exhibited the best antimicrobial activity, and for the higher generation compound **1-G4**, both at 1.0 mg/mL (Fig. S3). The **1-G2** was found to be dispersed in water as unimers, with an average hydrodynamic diameter (D_h) of 0.7 ± 0.1 nm, indicating that it remains solubilized at MIC values (far from the used for the DLS study), exhibiting an antibiotic-like behavior. In contrast, **1-G4** self-assembled into micelles (D_h = 41 ± 17 nm) with a spherical morphology according to TEM (Fig. S3b). The CAC of this dendron was determined to be 98 μg/mL, which is of the same order of magnitude as its MIC. Therefore, this suggests that the antimicrobial activity is related to the self-assembly of this higher generation dendron [34].

In conclusion, the antimicrobial efficacy of these dendronized macromolecules is governed by both the length of the alkyl chain and the number of cationic moieties present. These molecular characteristics influence the physicochemical interactions with bacterial membranes, thereby modulating surface affinity and determining the overall efficiency of bacterial adhesion and membrane disruption.

To elucidate whether the mechanism of action of the short alkyl chain dendritic macromolecules (**1-Gn**), those that exhibited the highest bactericidal activity, was directed towards the bacterial membrane via electrostatic interactions, SEM images were taken on bacterial cells before and after treatment with MICs for each compound. Remarkable differences were observed in the cellular membranes of both bacterial strains before and after treatment (Fig. 2). In untreated bacteria, *S. aureus* exhibited a characteristic spherical morphology with smooth, intact membranes, while *E. coli* showed the expected rod-shaped morphology with undamaged membranes. In contrast, treated bacteria exhibited severe membrane damage, including the appearance of surface disruptions, dents, pore formation, and deformation of the typical bacterial shape. The degree of morphological damage appeared correlated with the antimicrobial activity observed in our prior assays, suggesting that membrane disruption is one mechanism of antimicrobial action for these linear-dendritic macromolecules, as previously reported for other guanidinium-derived compounds [36]. The damage across both Gram-positive and Gram-negative strains indicates a

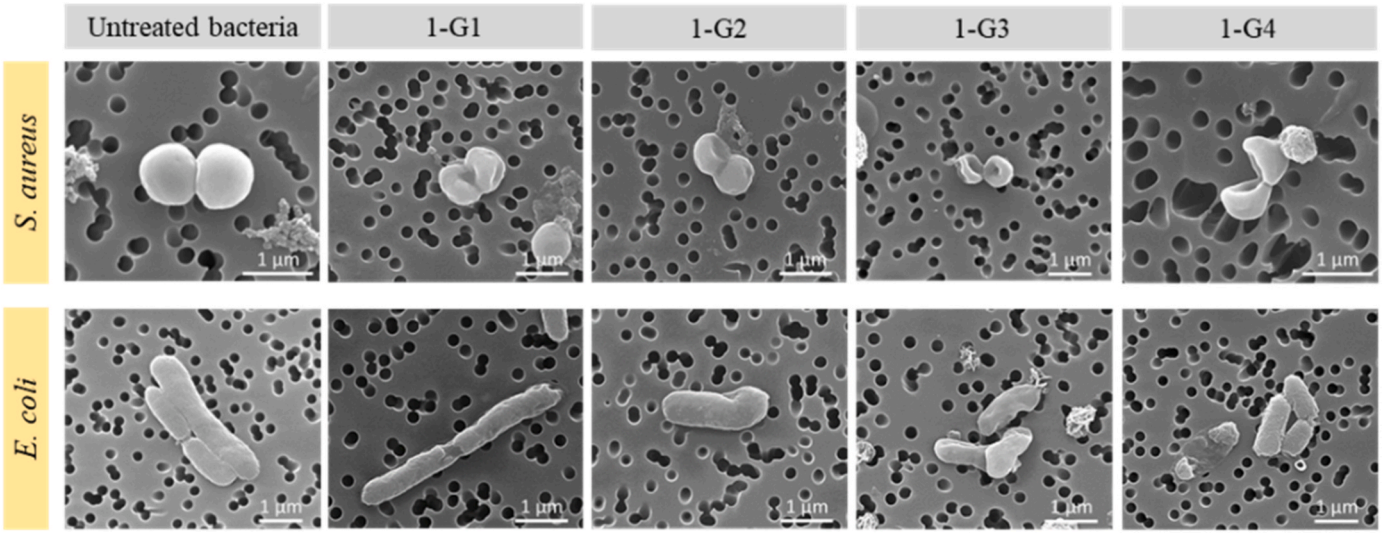

Fig. 2. SEM images of *S. aureus* (top) and *E. coli* (bottom) before treatment and after treatment with MIC values of **1-G1**, **1-G2**, **1-G3** and **1-G4** compounds.

broad-spectrum of antimicrobial action which represents a positive outcome to reduce antimicrobial resistance and to initially treat unknown infections and polymicrobial ones.

3.3. Cytotoxicity study

Given the importance of ensuring biosafety of antibacterial agents toward eukaryotic cells, cytotoxicity studies of all the cationic linear-dendritic macromolecules were performed in human dermal fibroblast, HaCaT human keratinocytes and J774A.1 mouse monocyte-macrophages. According to the ISO 10993–5:2009 standard [51], a medical device is deemed cytocompatible if it maintains cell viability above 70 %. As shown in Fig. 3e–h, all long-chain dendritic compounds, **2-Gn**, exhibited cytotoxicity at concentrations above 20 μg/mL. Given that the MICs for both *S. aureus* and *E. coli* exceed these cytotoxic levels, these compounds would not be suitable for antibacterial applications that require preservation of mammalian cell viability. In contrast, promising outcomes were observed when short-chain dendritic compounds, **1-Gn**, were evaluated in eukaryotic cells. Among these, both **1-G3** and **1-G4** dendrons displayed cytotoxicity at concentrations equivalent to the MICs for both bacterial strains (100 and 10 μg/mL for *S. aureus* and 20 and 5 μg/mL for *E. coli*, respectively), indicating limited biocompatibility at therapeutically relevant antimicrobial doses (Fig. 3c and d). Notably, the **1-G2** dendron (Fig. 3b) demonstrated high cytocompatibility with the eukaryotic cell lines tested at its MIC value (2.5 μg/mL for both *S. aureus* and *E. coli*). Furthermore, **1-G2** maintained excellent cytocompatibility even at its MBC of 5 μg/mL for both strains, suggesting that this antibiotic-like compound is a highly promising candidate for antibacterial applications without compromising mammalian cell viability. Finally, **1-G1** compound also showed good cytocompatibility at MIC and MBC values for *S. aureus* (2.5 and 20 μg/mL, respectively). However, for *E. coli*, a reduction in cellular viability was observed at the MBC (50 μg/mL), falling below the 70 % of viability threshold, indicating some cytotoxicity at high concentrations.

According to the SI values calculated and presented in Table 2, the dendritic compound **1-G1** is an effective, highly reliable, and safe therapy against Gram-positive bacteria, as Table 2 shows the highest SI values. This means that it would be therapeutically effective against *S. aureus* infection but without affecting the viability of mammalian cells and it could also be considered as an "antibiotic-like" compound selective for Gram-positive bacteria. On the other hand, it is also worth noting that compound **1-G2** is the only dendron that consistently exhibits SI values greater than 1 across all evaluated cell lines. This clearly indicates that **1-G2** retains its antimicrobial efficacy at concentrations that do not induce significant toxicity in mammalian cells, reinforcing its antibiotic-like behavior. In practical terms, **1-G2** is able to selectively target bacterial cells while sparing host cells, demonstrating a desirable balance between potency and safety. Therefore, the SI data strongly support the potential of **1-G2** as a promising antibacterial candidate with reduced risk of adverse effects on mammalian cells, making it an attractive lead for further optimization and in-depth preclinical evaluation.

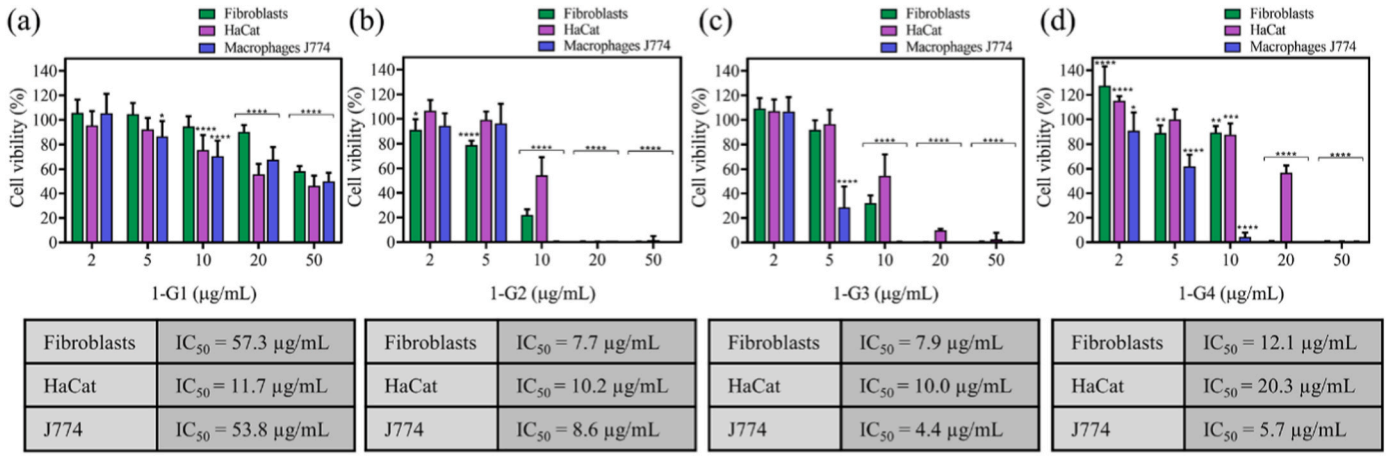

Fibroblasts	IC_{50} = 57.3 μg/mL
HaCat	IC_{50} = 11.7 μg/mL
J774	IC_{50} = 53.8 μg/mL

Fibroblasts	IC_{50} = 7.7 μg/mL
HaCat	IC_{50} = 10.2 μg/mL
J774	IC_{50} = 8.6 μg/mL

Fibroblasts	IC_{50} = 7.9 μg/mL
HaCat	IC_{50} = 10.0 μg/mL
J774	IC_{50} = 4.4 μg/mL

Fibroblasts	IC_{50} = 12.1 μg/mL
HaCat	IC_{50} = 20.3 μg/mL
J774	IC_{50} = 5.7 μg/mL

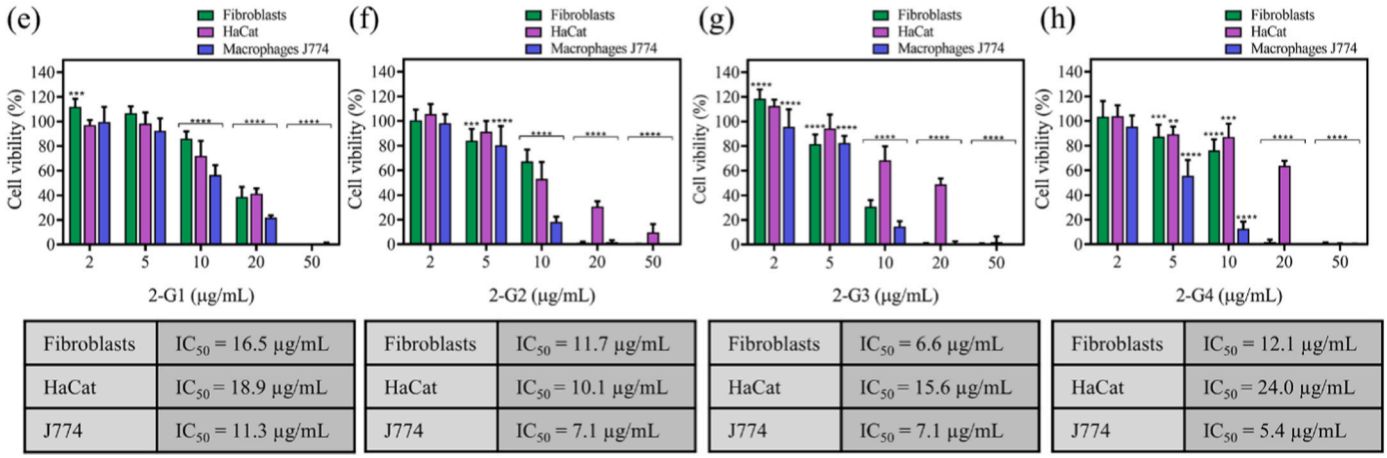

Fibroblasts	IC_{50} = 16.5 μg/mL
HaCat	IC_{50} = 18.9 μg/mL
J774	IC_{50} = 11.3 μg/mL

Fibroblasts	IC_{50} = 11.7 μg/mL
HaCat	IC_{50} = 10.1 μg/mL
J774	IC_{50} = 7.1 μg/mL

Fibroblasts	IC_{50} = 6.6 μg/mL
HaCat	IC_{50} = 15.6 μg/mL
J774	IC_{50} = 7.1 μg/mL

Fibroblasts	IC_{50} = 12.1 μg/mL
HaCat	IC_{50} = 24.0 μg/mL
J774	IC_{50} = 5.4 μg/mL

Fig. 3. Cytotoxicity and IC_{50} values in human dermal fibroblasts, HaCaT human keratinocytes and J774A.1 mouse monocyte-macrophages of the cationic linear-dendritic macromolecules: **(a) 1-G1**, **(b) 1-G2**, **(c) 1-G3**, **(d) 1-G4**, **(e) 2-G1**, **(f) 2-G2**, **(g) 2-G3** and **(h) 2-G4**. Results are presented as mean ± standard deviation. At least three independent replicates were performed in triplicate. 100 % viability was assigned to untreated controls. Statistically significant differences between the non-treated and treated cells (*$p < 0.05$; **$p < 0.01$; ***$p < 0.001$; ****$p < 0.0001$) are also depicted.

Table 2
Selectivity index (SI) values for all dendrons against the different bacterial strains (*S. aureus* and *E. coli*), calculated based on their IC_{50} values for each cell line (human dermal fibroblasts, HaCaT human keratinocytes and J774A.1 mouse monocyte-macrophages). Values lower than 1 indicate poor selectivity, meaning the compound is more toxic to mammalian cells than to bacteria.

Dendron	Selectivity Index (SI)					
	S. aureus ATCC 25923			*E. coli* S17 (Gram-negative)		
	Fibroblasts	*HaCat*	*J774*	*Fibroblasts*	*HaCat*	*J774*
1-G1	22.9	4.7	21.5	2.9	<1	2.7
1-G2	3.1	4.1	3.4	1.5	2.0	1.7
1-G3	<1	1	<1	<1	<1	<1
1-G4	<1	<1	<1	<1	<1	<1
2-G1	<1	<1	<1	<1	<1	<1
2-G2	<1	<1	<1	<1	<1	<1
2-G3	<1	<1	<1	<1	<1	<1
2-G4	<1	<1	<1	<1	<1	<1

4. Conclusions

With orthogonal click chemistry, a series of bis-MPA based linear-dendritic structures functionalized with peripheral cationic guanidinium groups has been synthesized. This synthetic strategy allows for easy access to cationic dendrons and facilitates the tuning of different structural parameters from a single dendritic scaffold, such as the type of focal aliphatic chain. The dendritic generation and length of the focal aliphatic chain of these guanidinium-dendrons has a significant impact on antimicrobial activity. The dendrons attached to the short alkyl chains show superior bactericidal properties compared to those with longer chains. Specifically, the second-generation dendron, **1-G2**, owns the most potent antimicrobial activity while maintaining high cytocompatibility with eukaryotic cell lines, likely due to an optimal number of guanidinium groups and an adequate hydrophobic/hydrophilic balance. Moreover, the SI values clearly identify **1-G1** as the safest dendron for the treatment of Gram-positive bacterial infections (*S. aureus*) and the compound **1-G2** as the most promising candidate for Gram-positive and Gram-negative associated infections, as it maintains antibacterial activity at concentrations that remain non-toxic to mammalian cells. Therefore, this dendritic structure has the potential to behave as an antibiotic-like compound. Moreover, their non-selective mechanism of antimicrobial action against both Gram-positive and Gram-negative bacteria, targeting their membranes, is a promising feature to minimize the risk of resistance development.

CRediT authorship contribution statement

Javier Martín-Martín: Writing – original draft, Visualization, Investigation. **Sara Bescós-Ramo:** Writing – review & editing, Investigation. **Almudena Terrel:** Investigation. **Manuel Arruebo:** Writing – review & editing, Supervision, Resources, Funding acquisition. **Milagros Piñol:** Writing – review & editing, Supervision, Resources, Funding acquisition. **Cristina Yus:** Writing – review & editing, Writing – original draft, Methodology, Investigation. **Luis Oriol:** Writing – review & editing, Supervision, Project administration, Funding acquisition, Conceptualization.

Declaration of competing interest

The authors declare that they have no known competing financial interests or personal relationships that could have appeared to influence the work reported in this paper.

Acknowledgments

This work was financially supported by MICIN/AEI (PDI2021-1261132NB-I00, PID2023-146091OB-I00 and PID2024-157398NB-I00) and Gobierno de Aragón-FSE (LMP93_21 and E47_23R). INMA authors acknowledge grant CEX2023-001286-S funded by MICIU/AEI/10.13039/501100011033. JMM acknowledges MICIN/AEI his FPI PhD grant and SBR her Gobierno de Aragón PhD grant. Authors would like to acknowledge the use of Servicio General de Apoyo a la Investigación-SAI, Universidad de Zaragoza, NAMBIOSIS and ELECMI-Laboratorio de Microscopías Avanzadas-LMA (INMA-Unizar) and Servicios Científicos Técnicos of CEQMA (CSIC-Unizar). CSIC-Conexión Nanomedicina is also acknowledged.

Appendix A. Supplementary data

Supplementary data to this article can be found online at https://doi.org/10.1016/j.mtchem.2025.103342.

Data availability

Data will be made available on request.

References

[1] M.I. Hutchings, A.W. Truman, B. Wilkinson, Antibiotics: past, present and future, Curr. Opin. Microbiol. 51 (2019) 72–80, https://doi.org/10.1016/j.mib.2019.10.008.
[2] K.M.G. O'Connell, J.T. Hodgkinson, H.F. Sore, M. Welch, G.P.C. Salmond, D. R. Spring, Combating multidrug-resistant bacteria: current strategies for the discovery of novel antibacterials, Angew. Chem. Int. Ed. 52 (2013) 10706–10733, https://doi.org/10.1002/anie.201209979.
[3] K.E. Jones, N.G. Patel, M.A. Levy, A. Storeygard, D. Balk, J.L. Gittleman, P. Daszak, Global trends in emerging infectious diseases, Nature 451 (2008) 990–993, https://doi.org/10.1038/nature06536.
[4] N. Mookherjee, M.A. Anderson, H.P. Haagsman, D.J. Davidson, Antimicrobial host defence peptides: functions and clinical potential, Nat. Rev. Drug Discov. 19 (2020) 311–332, https://doi.org/10.1038/s41573-019-0058-8.
[5] A. Bahar, D. Ren, Antimicrobial peptides, Pharmaceuticals 6 (2013) 1543–1575, https://doi.org/10.3390/ph6121543.
[6] C.D. Fjell, J.A. Hiss, R.E.W. Hancock, G. Schneider, Designing antimicrobial peptides: form follows function, Nat. Rev. Drug Discov. 11 (2012) 37–51, https://doi.org/10.1038/nrd3591.
[7] W. Shen, P. He, C. Xiao, X. Chen, From antimicrobial peptides to antimicrobial Poly (α -amino acid)s, Adv. Healthcare Mater. 7 (2018) 1800354, https://doi.org/10.1002/adhm.201800354.
[8] J. Wang, X. Dou, J. Song, Y. Lyu, X. Zhu, L. Xu, W. Li, A. Shan, Antimicrobial peptides: promising alternatives in the post feeding antibiotic era, Med. Res. Rev. 39 (2019) 831–859, https://doi.org/10.1002/med.21542.
[9] B.H. Gan, J. Gaynord, S.M. Rowe, T. Deingruber, D.R. Spring, The multifaceted nature of antimicrobial peptides: current synthetic chemistry approaches and future directions, Chem. Soc. Rev. 50 (2021) 7820–7880, https://doi.org/10.1039/D0CS00729C.
[10] R.E.W. Hancock, H.-G. Sahl, Antimicrobial and host-defense peptides as new anti-infective therapeutic strategies, Nat. Biotechnol. 24 (2006) 1551–1557, https://doi.org/10.1038/nbt1267.
[11] M. Mahlapuu, J. Håkansson, L. Ringstad, C. Björn, Antimicrobial peptides: an emerging category of therapeutic agents, Front. Cell. Infect. Microbiol. 6 (2016), https://doi.org/10.3389/fcimb.2016.00194.
[12] P. Pham, S. Oliver, C. Boyer, Design of antimicrobial polymers, Macromol. Chem. Phys. 224 (2023) 2200226, https://doi.org/10.1002/macp.202200226.
[13] K. Kuroda, W.F. DeGrado, Amphiphilic polymethacrylate derivatives as antimicrobial agents, J. Am. Chem. Soc. 127 (2005) 4128–4129, https://doi.org/10.1021/ja044205+.
[14] L.M. Thoma, B.R. Boles, K. Kuroda, Cationic methacrylate polymers as topical antimicrobial agents against *Staphylococcus aureus* nasal colonization, Biomacromolecules 15 (2014) 2933–2943, https://doi.org/10.1021/bm500557d.
[15] F. Nederberg, Y. Zhang, J.P.K. Tan, K. Xu, H. Wang, C. Yang, S. Gao, X.D. Guo, K. Fukushima, L. Li, J.L. Hedrick, Y.-Y. Yang, Biodegradable nanostructures with selective lysis of microbial membranes, Nat. Chem. 3 (2011) 409–414, https://doi.org/10.1038/nchem.1012.
[16] W. Chin, G. Zhong, Q. Pu, C. Yang, W. Lou, P.F. De Sessions, B. Periaswamy, A. Lee, Z.C. Liang, X. Ding, S. Gao, C.W. Chu, S. Bianco, C. Bao, Y.W. Tong, W. Fan, M. Wu, J.L. Hedrick, Y.Y. Yang, A macromolecular approach to eradicate multidrug resistant bacterial infections while mitigating drug resistance onset, Nat. Commun. 9 (2018) 917, https://doi.org/10.1038/s41467-018-03325-6.
[17] Z.-Y. Li, X. Zhang, Y.-L. Qian, F.-S. Du, Z.-C. Li, Synthesis and antibacterial properties of fluorinated biodegradable cationic polyesters, J. Mater. Chem. B 12 (2024) 1569–1578, https://doi.org/10.1039/D3TB02578K.
[18] E.F. Palermo, K. Kuroda, Chemical structure of cationic groups in amphiphilic polymethacrylates modulates the antimicrobial and hemolytic activities, Biomacromolecules 10 (2009) 1416–1428, https://doi.org/10.1021/bm900044x.
[19] L. Martin, R. Peltier, A. Kuroki, J.S. Town, S. Perrier, Investigating cell uptake of guanidinium-rich RAFT polymers: impact of comonomer and monomer

distribution, Biomacromolecules 19 (2018) 3190–3200, https://doi.org/10.1021/acs.biomac.8b00146.
[20] K.E.S. Locock, T.D. Michl, J.D.P. Valentin, K. Vasilev, J.D. Hayball, Y. Qu, A. Traven, H.J. Griesser, L. Meagher, M. Haeussler, Guanylated polymethacrylates: a class of potent antimicrobial polymers with low hemolytic activity, Biomacromolecules 14 (2013) 4021–4031, https://doi.org/10.1021/bm401128r.
[21] K. Kuroda, G.A. Caputo, W.F. DeGrado, The role of hydrophobicity in the antimicrobial and hemolytic activities of polymethacrylate derivatives, Chem. Eur J. 15 (2009) 1123–1133, https://doi.org/10.1002/chem.200801523.
[22] E.F. Palermo, K. Kuroda, Structural determinants of antimicrobial activity in polymers which mimic host defense peptides, Appl. Microbiol. Biotechnol. 87 (2010) 1605–1615, https://doi.org/10.1007/s00253-010-2687-z.
[23] C. Ergene, K. Yasuhara, E.F. Palermo, Biomimetic antimicrobial polymers: recent advances in molecular design, Polym. Chem. 9 (2018) 2407–2427, https://doi.org/10.1039/C8PY00012C.
[24] S. Alfei, A.M. Schito, From nanobiotechnology, positively charged biomimetic dendrimers as novel antibacterial agents: a review, Nanomaterials 10 (2020) 2022, https://doi.org/10.3390/nano10102022.
[25] M. Grillaud, J. Russier, A. Bianco, Polycationic adamantane-based dendrons of different generations display high cellular uptake without triggering cytotoxicity, J. Am. Chem. Soc. 136 (2014) 810–819, https://doi.org/10.1021/ja411987g.
[26] E. Fuentes-Paniagua, J. Sánchez-Nieves, J.M. Hernández-Ros, A. Fernández-Ezequiel, J. Soliveri, J.L. Copa-Patiño, R. Gómez, F. Javier De La Mata, Structure–activity relationship study of cationic carbosilane dendritic systems as antibacterial agents, RSC Adv. 6 (2016) 7022–7033, https://doi.org/10.1039/C5RA25901K.
[27] O.C.J. Andrén, T. Ingverud, D. Hult, J. Håkansson, Y. Bogestål, J.S. Caous, K. Blom, Y. Zhang, T. Andersson, E. Pedersen, C. Björn, P. Löwenhielm, M. Malkoch, Antibiotic-free cationic dendritic hydrogels as surgical-site-infection-inhibiting coatings, Adv. Healthcare Mater. 8 (2019) 1801619, https://doi.org/10.1002/adhm.201801619.
[28] W. Guo, Y. Wang, P. Wan, H. Wang, L. Chen, S. Zhang, C. Xiao, X. Chen, Cationic amphiphilic dendrons with effective antibacterial performance, J. Mater. Chem. B 10 (2022) 456–467, https://doi.org/10.1039/D1TB02037D.
[29] D. Huang, D. Wu, Biodegradable dendrimers for drug delivery, Mater. Sci. Eng. C 90 (2018) 713–727, https://doi.org/10.1016/j.msec.2018.03.002.
[30] P. Stenström, E. Hjorth, Y. Zhang, O.C.J. Andrén, S. Guette-Marquet, M. Schultzberg, M. Malkoch, Synthesis and *In vitro* evaluation of Monodisperse amino-functional polyester dendrimers with rapid degradability and antibacterial properties, Biomacromolecules 18 (2017) 4323–4330, https://doi.org/10.1021/acs.biomac.7b01364.
[31] F. Namata, N. Sanz Del Olmo, N. Molina, M. Malkoch, Synthesis and characterization of amino-functional polyester dendrimers based on Bis-MPA with enhanced hydrolytic stability and inherent antibacterial properties, Biomacromolecules 24 (2023) 858–867, https://doi.org/10.1021/acs.biomac.2c01286.
[32] I. Heredero-Bermejo, J.M. Hernández-Ros, L. Sánchez-García, M. Maly, C. Verdú-Expósito, J. Soliveri, F. Javier de la Mata, J.L. Copa-Patiño, J. Pérez-Serrano, J. Sánchez-Nieves, R. Gómez, Ammonium and guanidine carbosilane dendrimers and dendrons as microbicides, Eur. Polym. J. 101 (2018) 159–168, https://doi.org/10.1016/j.eurpolymj.2018.02.025.
[33] C. Galanakou, D. Dhumal, L. Peng, Amphiphilic dendrimers against antibiotic resistance: light at the end of the tunnel? Biomater. Sci. 11 (2023) 3379–3393, https://doi.org/10.1039/D2BM01878K.
[34] D. Dhumal, B. Maron, E. Malach, Z. Lyu, L. Ding, D. Marson, E. Laurini, A. Tintaru, B. Ralahy, S. Giorgio, S. Pricl, Z. Hayouka, L. Peng, Dynamic self-assembling supramolecular dendrimer nanosystems as potent antibacterial candidates against drug-resistant bacteria and biofilms, Nanoscale 14 (2022) 9286–9296, https://doi.org/10.1039/D2NR02305A.
[35] A. Chen, A. Karanastasis, K.R. Casey, M. Necelis, B.R. Carone, G.A. Caputo, E. F. Palermo, Cationic molecular umbrellas as antibacterial agents with remarkable cell-type selectivity, ACS Appl. Mater. Interfaces 12 (2020) 21270–21282, https://doi.org/10.1021/acsami.9b19076.
[36] A. Chen, E. Chen, E.F. Palermo, Guanidium-functionalized cationic molecular umbrellas as antibacterial agents, Polym. Chem. 12 (2021) 2374–2378, https://doi.org/10.1039/D1PY00071C.
[37] T.N. Siriwardena, M. Stach, R. He, B.-H. Gan, S. Javor, M. Heitz, L. Ma, X. Cai, P. Chen, D. Wei, H. Li, J. Ma, T. Köhler, C. Van Delden, T. Darbre, J.-L. Reymond, Lipidated peptide dendrimers killing multidrug-resistant bacteria, J. Am. Chem. Soc. 140 (2018) 423–432, https://doi.org/10.1021/jacs.7b11037.
[38] Z. Lai, Q. Jian, G. Li, C. Shao, Y. Zhu, X. Yuan, H. Chen, A. Shan, Self-assembling peptide dendron nanoparticles with high stability and a multimodal antimicrobial mechanism of action, ACS Nano 15 (2021) 15824–15840, https://doi.org/10.1021/acsnano.1c03301.
[39] N. King, D. Dhumal, S.Q. Lew, S.H. Kuo, C. Galanakou, M.W. Oh, S.Y. Chong, N. Zhang, L.T.O. Lee, Z. Hayouka, L. Peng, G.W. Lau, Amphiphilic dendrimer as potent antibacterial against drug-resistant bacteria in mouse models of human infectious diseases, ACS Infect. Dis. 10 (2024) 453–466, https://doi.org/10.1021/acsinfecdis.3c00425.
[40] N. Zhang, D. Dhumal, S.H. Kuo, S.Q. Lew, P.D. Patil, R. Taher, S. Vaidya, C. Galanakou, A. Elkihel, M.W. Oh, S.Y. Chong, D. Marson, J. Zheng, O. Rouvinski, W.O. Abolarin, S. Pricl, G.W. Lau, L.T.O. Lee, L. Peng, Targeting the phosphatidylglycerol lipid: an amphiphilic dendrimer as a promising antibacterial candidate, Sci. Adv. 10 (2024) eadn8117, https://doi.org/10.1126/sciadv.adn8117.
[41] Y. Fan, S. Mohanty, Y. Zhang, M. Lüchow, L. Qin, L. Fortuin, A. Brauner, M. Malkoch, Dendritic hydrogels induce immune modulation in human keratinocytes and effectively eradicate bacterial pathogens, J. Am. Chem. Soc. 143 (2021) 17180–17190, https://doi.org/10.1021/jacs.1c07492.
[42] N. Sanz Del Olmo, N. Molina, Y. Fan, F. Namata, D.J. Hutchinson, M. Malkoch, Antibacterial hydrogel adhesives based on bifunctional telechelic dendritic-Linear–Dendritic block copolymers, J. Am. Chem. Soc. 146 (2024) 17240–17249, https://doi.org/10.1021/jacs.4c03673.
[43] P. Antoni, M.J. Robb, L. Campos, M. Montanez, A. Hult, E. Malmström, M. Malkoch, C.J. Hawker, Pushing the limits for thiol−Ene and CuAAC reactions: synthesis of a 6th generation dendrimer in a single day, Macromolecules 43 (2010) 6625–6631, https://doi.org/10.1021/ma101242u.
[44] E. Blasco, J. del Barrio, M. Piñol, L. Oriol, C. Berges, C. Sánchez, R. Alcalá, Azobenzene-containing linear–dendritic block copolymers prepared by sequential ATRP and click chemistry, Polymer 53 (2012) 4604–4613, https://doi.org/10.1016/j.polymer.2012.08.022.
[45] S. García-Gallego, D. Hult, J.V. Olsson, M. Malkoch, Fluoride-promoted esterification with imidazolide-activated compounds: a modular and sustainable approach to dendrimers, Angew. Chem. Int. Ed. 54 (2015) 2416–2419, https://doi.org/10.1002/anie.201411370.
[46] Azides and Nitrenes, Reactivity and Utility, Academic Press, 1984, pp. 205–246.
[47] M.J. Little, N. Aubry, M.-E. Beaudoin, N. Goudreau, S.R. LaPlante, Quantifying trifluoroacetic acid as a counterion in drug discovery by ^{19}F NMR and capillary electrophoresis, J. Pharm. Biomed. Anal. 43 (2007) 1324–1330, https://doi.org/10.1016/j.jpba.2006.10.039.
[48] Z. Deng, R. Zhang, J. Gong, Z. Zhang, L. Zhang, Z. Qiu, P. Alam, J. Zhang, Y. Liu, Y. Li, Z. Zhao, B.Z. Tang, Unveiling the role of alkyl chain in boosting antibacterial selectivity and cell biocompatibility, JACS Au 5 (2025) 675–683, https://doi.org/10.1021/jacsau.4c00915.
[49] N. Hanheiser, Y. Jiang, C. Zoister, M. Dimde, K. Achazi, C. Nie, Y. Li, R. Haag, A. K. Singh, Modular synthesis of dendritic oligo-glycerol cationic surfactants for enhanced antibacterial efficacy, Angew. Chem. Int. Ed. 64 (2025) e202425069, https://doi.org/10.1002/anie.202425069.
[50] X. Luo, Z. Jiang, N. Zhang, Z. Yang, Z. Zhou, Interactions of biocidal polyhexamethylene guanidine hydrochloride and its analogs with POPC model membranes, Polymers 9 (2017) 517, https://doi.org/10.3390/polym9100517.
[51] Biological evaluation of medical devices —part 5: tests for *In Vitro* cytotoxicity, in: ANSI/AAMI/ISO 10993-5:2009/(R)2014; Biological Evaluation of Medical Devices —Part 5: Tests for in Vitro Cytotoxicity, AAMI, 2009, https://doi.org/10.2345/9781570203558.ch1.